

Exploring Extended Sources with VERITAS



Jack Dickson^{a,b}

^aUniversity of California, Los Angeles ^bNevis Laboratories, Columbia University

Abstract

The Large High Altitude Air Shower Observatory (LHAASO) recently published a catalog introducing several new γ -ray sources at Very High Energy (VHE) and Ultra High Energy (UHE) levels. Some of these sources are promising "PeVatron" candidates that require further examination within the tera-electronvolt (TeV) range. Predominantly, these high-energy sources are extended sources. This paper aims to provide foundational knowledge on the analysis of γ -ray sources with Imaging Atmospheric Cherenkov Telescopes (IACTs). Furthermore, it aims to investigate how the Very Energetic Radiation Imaging Telescope Array System (VER-ITAS) can examine these extended sources by assessing how the VERITAS software package, VEGAS, estimates the background for extended source exclusion regions. This study used data from both the Crab Nebula and the quasar 3C 273 to test various exclusion regions, creating corresponding maps to represent background estimation. Findings from the study indicate that while background estimation remains consistent for exclusion regions below 0.9°, it needs refinement for regions of approximately 0.9° in order to facilitate further analysis.

Contents

1	Intr	roduction	1
	1.1	Cosmic Rays	1
	1.2		2
	1.3	Air Shower Astronomy	2
		VERITAS (Detector)	3
		LHAASO (Detector)	3
	1.6	LHAASO J1857+0203u	3
2	Bac	kground Estimation	4
	2.1	Ring Background Method	4
	2.2		4
	2.3	VEGAS (Analysis Software)	4
3	Results: Validation of the background method using the Crab and quasar 3C 273 data		
	3.1	Results of validation with the Crab	5
	3.2	Results of validation with quasar 3C 273	7
4	Disc	cussion	8
5	Sun	nmary and conclusions	8
A	ppen	ndix A More Plots	8

1. Introduction

Gamma (γ) ray astronomy studies the highest energies of the electromagnetic spectrum above 100 KeV. γ -rays are made in non-thermal processes making the events which produced them extremely violent. γ -ray astronomy explores these events in the

universe such as the areas around black-holes and active galactic nuclei (AGN). γ -ray astronomy also probes dark matter and phenomena that violate Lorentz invariance, both unanswered questions in modern physics. The analysis this paper will focus on is based upon two detectors, VERITAS (Very Energetic Radiation Imaging Telescope Array System) and LHAASO (Large High Altitude Air Shower Observatory). Up until this year, only around 200 γ -ray sources above 100GeV had been detected, but the new LHAASO detector has enabled another 32 VHE (Very High Energy) and 43 UHE (Ultra High Energy) γ -ray sources to be detected [1]. Among these LHAASO sources is J1857+0203u which is previously detected coincident with a radio structure resembling a superbubble [7]. The motivation for this paper and REU project is to understand the physics behind this source using VERITAS data.

1.1. Cosmic Rays

Cosmic Rays are charged particles that through various mechanisms reach relativistic speeds. The observed cosmic rays are made up of approximately 92% protons, 6% helium, 1% electrons and 1% heavier nucluei [5]. The spectrum of these cosmic rays is very well documented, as seen in Figure 1. The energies of cosmic rays span from 10⁷ eV all the way up to 10²⁰ eV, with the flux of cosmic rays declining the higher energy they have. The highest energies of cosmic rays are of interest to astrophysicists because the mechanisms upon which they are accelerated are extremely violent. The physics of high energy cosmic ray acceleration is the physics of the most violent parts of the universe. The cosmological objects that can create these extreme conditions in which the highest energy cosmic rays are created are called "PeVatrons." PeVatrons can

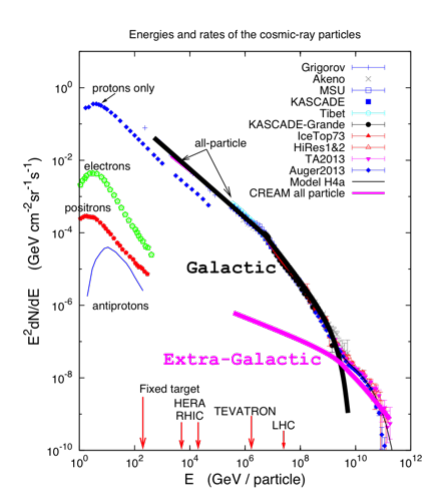


Figure 1: The flux-energy spectrum of cosmic rays. In the figure the current data as well as best fit models are shown. The figure is in a log log scale which means that the spectrum of cosmic rays follows a power law spectrum with the highest energies falling off very quickly in flux.

accelerate charged particles up to the Peta-Electron Volt (PeV or $10^{15} \mathrm{eV}$) energy range. Even though the detection of these cosmic rays is well known and documented, the acceleration mechanism of cosmic rays and the site of the acceleration are still unclear. Cosmic rays can produce γ -rays by interacting with ambient material. Because γ -rays are charge neutral, they are not deflected by the interstellar magnetic fields and allow for physicists to study the sites of cosmic ray acceleration.

1.2. γ-ray Production

High energy γ -rays are produced by a number of different mechanisms but the two distinctions can be from either leptonic origin or hadronic origin, both of which are non-thermal.

The leptonic origin for γ -rays stems from the fact that they are made by processes involving an electron. These can be either synchrotron radiation or inverse Compton scattering. In synchrotron radiation, the electron is accelerated in a helical path which produces radiation, often in the X-ray spectrum. Inverse Compton scattering refers to the process in which a photon and a relativistic electron collide and the electron up scatters the photon resulting in a γ -ray being created

$$\gamma + e^{-} \rightarrow e^{-'} + \gamma' \tag{1}$$

where γ' is of higher energy. For example, Figure 2 shows the process of inverse Compton scattering.

The hadronic origin for γ -rays occurs when relativistic protons are the underlying particle that creates the γ -ray. This can happen when a fast moving proton collides with ambient gas in the galaxy. This process creates neutral pions (π^0). These pions then decay in the process

$$\pi^0 \to \gamma \gamma$$

where two γ -rays are created. Because the synthesis of γ -rays occurs by charged particles interacting with other particles,

Inverse Compton scattering

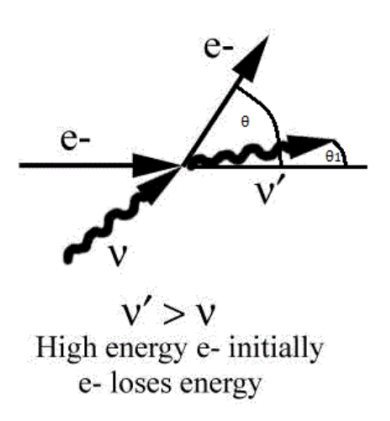


Figure 2: Diagram of how an incoming low energy photon scatters with a high energy electron and energy is transferred to the photon causing an up scattering of the photon and a higher energy γ -ray to be created in the process. Image Credit: venables.asu.edu/quant/proj/compton.html

the sites of cosmic ray acceleration should also produce γ -rays making them an ideal candidate for studying the areas of cosmic ray acceleration.

1.3. Air Shower Astronomy

As seen in Figure 1, the flux of cosmic rays follows a power law, with energy inversely related to flux. The low energy γ -rays can be detected by spaced-based detectors such as FERMILat. The low energy fluxes are higher which make the space-based γ -ray telescopes not need to be very large. However to see any higher energy γ -rays , the telescopes become too big to be economical in space. This requires physicists to use another technique for detecting cosmic rays and γ -rays, air shower detectors.

When an incoming γ -ray is incident with the atmosphere, it comes into contact with an atmospheric particle and pair production of an electron positron pair occurs from the recoil of the incident nucleus. Assuming a nucleus of atmosphere is nitrogen, the equation for which the critical energy of this pair production happens from an incident γ -ray is [6]

$$E_c = 2m_{nucleus}c^2 \approx 26.2GeV \tag{2}$$

These particles then radiate through a process called Bremsstrahlung in which the charged electron or positron is decelerated by another nucleus in the atmosphere [2]. This creates a cascade effect where more γ -rays are emitted that can create more pairs, as shown in Figure 3. When these high energy electrons move faster than the speed of light in air, they produce Cherenkov radiation and the resulting light cone is imaged by a Imaging Atmospheric Cherenkov Telescopes (IACTs) on the ground. The energy and the direction of the incoming γ -ray can be reconstructed using Hillas parameterization [8] of the γ -ray shower image. Both cosmic rays and γ -rays can cause Cherenkov light showers, but often it is possible to distinguish between them based upon how they cascade, with γ -ray air

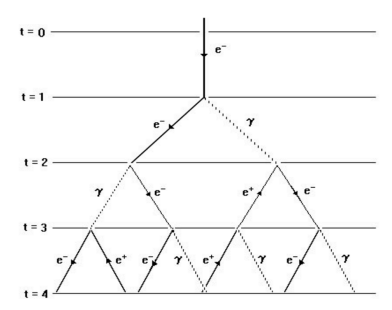


Figure 3: This graphic shows the pair production of e^- 's and e^+ 's when an incident γ -ray or cosmic ray hits a nucleus in the upper atmosphere and causes Bremsstrahlung, or brake radiation. The cascade occurs above the critical energy given by the equation $E_c = 2m_{nucleus}c^2$ and this production creates a light cone of Cherenkov radiation. [3]

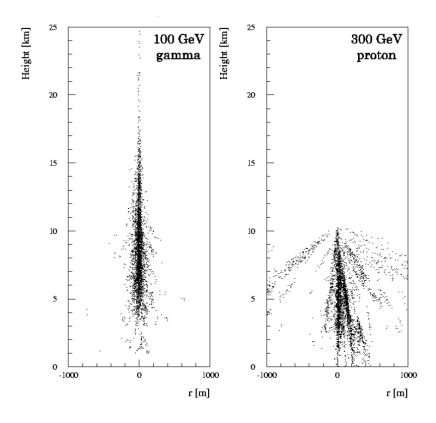


Figure 4: This graphic shows the difference in the air shower cascade based on whether the air shower was caused by a γ -ray or a cosmic ray. The left side shows γ -ray shower which cascades down in a narrow cone. The right side shows the cosmic ray shower which cascades down in a wider cone than the γ -ray. [3]

showers being much "skinnier" and less chaotic than cosmic ray air showers. This is because cosmic ray showers produce heavier pions which then deflect at larger angles. Figure 4 shows the visual differences between the air showers from γ -rays and cosmic rays.

1.4. VERITAS (Detector)

VERITAS is a ground based air shower γ -ray telescope located at the Whipple Observatory near Tucson Arizona. The array consists of four 12 meter Cherenkov telescopes that operate in the very high energy (VHE) band of γ -ray radiation (80GeV - 50TeV), however it performs best in its maximum sensitivity band of 100GeV - 10TeV. Each telescope consists of 499 "pixels" which are mirrors that reflect the incoming Cherenkov light into 499 photomultiplier tubes (PMTs). Those PMTs are then read out to the system when the necessary trigger levels occur. Since so much data is stored it is necessary to have some hard encoded triggers to filter out all the background from actual events. The data at VERITAS is taken in runs which are usually 30-40 minutes long. Because VERITAS has a high angular resolution, its total window size is small, around 3.5° so



Figure 5: The VERITAS building and telescopes at the Fred Lawrence Whipple Observatory (FLWO) in southern Arizona, USA. Image credit: VERITAS

these runs are specific targets in the night sky unlike other experiments like LHAASO or Fermi-LAT.

1.5. LHAASO (Detector)

LHAASO is a ground based air shower γ -ray detector but works in a different way than VERITAS. LHAASO is made up of three separate detector arrays but the current runs are only using two, the Water Cherenkov Detector Array (WCDA) and the kilometer squared muon and electron detector array (KM2A). The WCDA array works by burying many $36m^2$ water tanks underground. Each of these tanks have arrays of PMTs on the bottom and when incident relativistic particles travel through the tank, they emit Cherenkov radiation like an air shower detector. The KM2A detector is a large square kilometer array of muon and electron detectors, each around a square meter in size. These are also buried under ground to reduce background noise. Because the detectors are buried underground, the array has the advantage of being able to run constantly throughout the day. The angular resolution of LHAASO is much lower than VERITAS but the detector array makes up for this by having a much larger field of view (FOV). The WCDA operates in around the same energy regime as VERITAS, but the KM2A array operates in the ultra high energy (UHE) range, or > 1PeV. The new LHAASO catalog added a significant amount of new VHE and UHE γ -ray sources because of this large FOV and its ability to see extended sources. This is a large step forward because it indicates that the process in which high energy γ -rays and cosmic rays can take place over large areas of the sky, not just small compact objects.



Figure 6: The LHAASO detector array in Daocheng, Sichuan, China. Image credit: IHEP

1.6. LHAASO J1857+0203u

From the new LHAASO catalog, LHAASO identified a number of new sources that are connected with previously known sources, such as LHAASO J1857+0203u. This was found to

be connected to the source HESS J1857+026. J1857+026 was originally discovered by H.E.S.S (High Energy Stereoscopic System) in 2008 to be a very high emitting TeV γ -ray source that was extended. In 2014, MAGIC (Major Atmospheric Gamma Imaging Cherenkov Telescopes) did a detailed study and concluded that the emission from J1857+026 could be attributed to two separate sources right next each other. However, a new radio study by Petriella of J1857+026 discovered a superbubble coincident with the pulsar associated with J1857+026 [7]. A superbubble is a region of space that had its matter forcefully expelled by a supernova. The superbubble is shown in the radio data to be spatially coincident with the pulsar PSR J1856+0245 in Figure 7, giving evidence to the pulsar being the remnant of a supernova which created the superbubble. In Petriella's results, they claim that the pulsars interaction with the spatially coincident supperbubble could be the mechanism for the TeV emission of J1857+026. If this is the case, the physics surrounding γ -ray emission from interactions of a pulsar with a supperbubble pose a great target for VERITAS analysis.

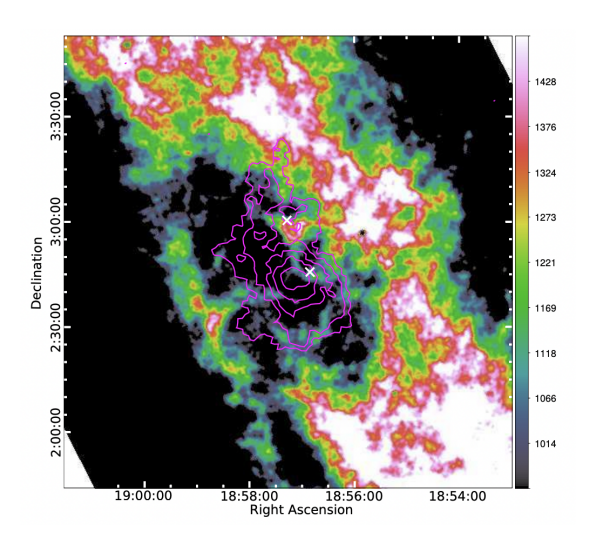


Figure 7: The radio data from Patriella's study. [7]

2. Background Estimation

In IACT astronomy, the dominant component of the background are cosmic ray events being misidentified as γ -ray events. In this study, Ring Background Method is used to predict the residual cosmic ray background.

2.1. Ring Background Method

Ring Background Method (RBM) estimates the background in a source by using the assumption that the background is axially symmetric around the optical axis and only depends on the angular distance to the optical axis. RBM draws a ring around the source region in question, often the center of the camera, and samples from this ring the background. The method assumes that this is γ -ray free data and uses this to create a curve

that corresponds to the background of the data. This curve decreases as the radius from the center of the camera increases due to the acceptance of the camera falling off with azimuthal angle. This background component is then used to subtract out the background from the γ -ray data.

2.2. Statistics (Li and Ma)

It is important to carefully study γ -ray data to make sure that the detection of a source is a true detection. In this study the statistics described in the Li and Ma paper is used to test the significance of the observed data [4]. Each given pixel in the camera has a number of counts N_c which corresponds the the number of on-counts N_{on} plus the number of off-counts N_{off} . These each correspond to the telescope looking at the source region versus looking at background through the "wobble" data collection mode. The wobble mode just moves the center of the telescope off of the source region to more accurately take background data. An estimated background counts \hat{N}_b is created using the equation

$$\hat{N}_b = \alpha N_{off} \tag{3}$$

The parameter α corresponds to the ratio between on and off times when taking data

$$\alpha = \frac{t_{on}}{t_{off}} \tag{4}$$

Using these total counts and background counts, it is then possible to test whether or not the data observed is a source or not. For the background, a Poissonian distribution is assumed. Using this assumption, the equation for the significance is

$$S = -\sqrt{2ln\lambda} = \sqrt{2} \left[N_{on} ln \left[\frac{1+\alpha}{\alpha} \left(\frac{N_{on}}{N_{on} + N_{off}} \right) \right] + N_{off} ln \left[(1+\alpha) \left(\frac{N_{off}}{N_{on} + N_{off}} \right) \right] \right]^{\frac{1}{2}}$$
(5)

This value of S corresponds to the number of standard deviations away from the norm an event is. This distribution follows a χ^2 distribution. This then allows for a significance of each pixel to be measured and mapped on a 2D significance map. A common lower value for a detection is taken to be S=5 which corresponds to 5 standard deviations away from the norm. The reason for using this common lower value is from the normal distribution, $S\sigma$ corresponds to an event that if background will happen around once in 10^6 trials or a 1 in a million chance.

2.3. VEGAS (Analysis Software)

To do analysis for this project, the software package VER-ITAS γ -ray Analysis Suite (VEGAS) was used to analyze the data. VEGAS is a software built on ROOT and Python by the VERITAS Collaboration that works to analyze data from VER-ITAS. VEGAS works in 6 stages to analyze the data from VER-ITAS.

• Stage 1: Collect data from VERITAS and calibrate the data using the corresponding "flasher runs" which are where a known emitter is flashed across the mirror to gauge the sensitivity for a given measurement.

- Stages 2/3: Take the calibrated data and subtract out all of the noise in the image. Each pixel is then cleaned and the entire image is smoothed to make the maps used for stages 4, 5, and 6.
- Stage 4: Take the now clean and smoothed image and find the Hillas parameters associated with that image. The include things like the size of the shower image and how far away the show image is from the center of the camera.
- Stage 5: Take the now cleaned images and Hillas parameters and create the root files which are then used to create the plots for stage 6.
- Stage 6: Create the maps and plots for the specific run.

3. Results: Validation of the background method using the Crab and quasar 3C 273 data

The purpose of this analysis is to validate how well the background estimation RBM works in VEGAS for extended sources. This is accomplished by using data taken of the Crab Nubula as well as the quasar 3C 273. Both of these γ -ray sources are point sources. In the observations of these sources no genuine γ -ray emission is expected in the field of view other than the location of the source. The data taken for both analysis are within the VERITAS telescope angles $58^{\circ} - 63^{\circ}$ to make sure the same angle of observation was consistent. The data that was used was made sure to have been good reliable data with all four telescopes running as well as the weather being amenable. 17.3 hours of data for both the Crab Nebula and the quasar 3C 273 were selected to have consistent amounts of data for both. Three different analysis regions (0.4°, 0.7°, 0.9°) were used for the Crab and four different analysis regions (0.3°, 0.5°, 0.7°, 0.9°) were used for 3C 273 to test how RBM is performing for different exclusion regions.

3.1. Results of validation with the Crab

Figures 8, 9, and 10 are the contrained significance maps of the Crab data. These are showing the significance of each pixel but only between a range of -5σ to 5σ so as to only show the background distribution of the data, which is important in the case of the Crab since it is the astronomers "standard candle" due to how bright it is. These figures show that the background model is not accounting for a lot of the background in the source exclusion region at a region of 0.9°. It is underestimating the background in these regions and causing the source to appear larger than it actually is. Looking at the 1-Dimensional plots, Figures 11, 12, and 13, of this significance this loss of background estimation at 0.9° can be seen. The significance plots should follow a nice gaussian fit, the blue curve, if the background is being estimated correctly. From the data, a 0.9° produces a plot that does not follow this nice gaussian curve. This is showing that the background estimation is failing.

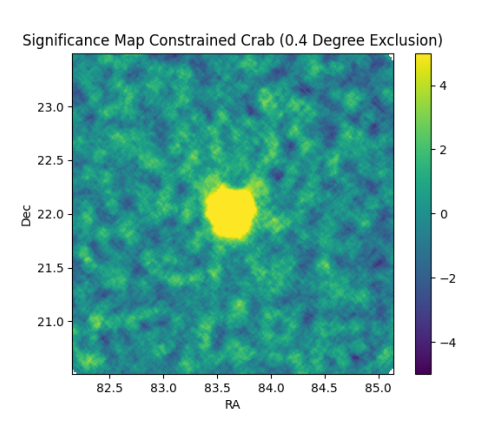


Figure 8: The Constrained Significance Map produced by VEGAS for the Crab Nebula with a 0.4° exclusion region. The fitted map shows that the background estimated around the source is mostly random with the source region being around the extent of The Crab. The color bar is showing the test significance and is not in any units, the x-axis and y-axis are in galactic rising angle and declination respectively.

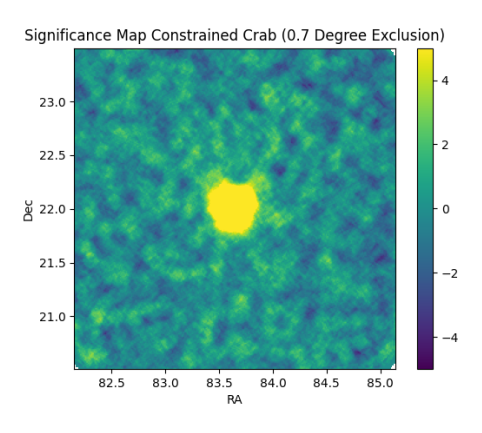


Figure 9: The Constrained Significance Map produced by VEGAS for the Crab Nebula with a 0.7° exclusion region. The fitted map shows that the background estimated around the source is mostly random with the source region being around the extent of The Crab. The color bar is showing the test significance and is not in any units, the x-axis and y-axis are in galactic rising angle and declination respectively.

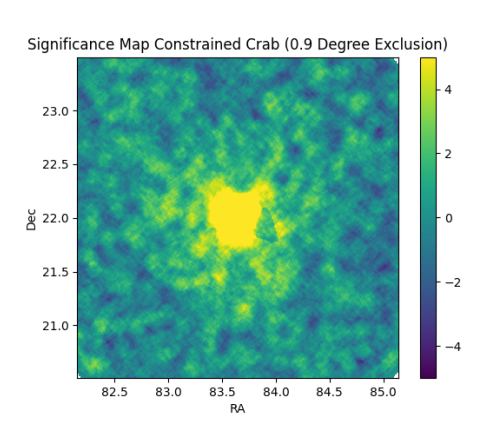


Figure 10: The Constrained Significance Map produced by VEGAS for the Crab Nebula with a 0.9° exclusion region. The fitted map shows that the background estimated around the source is mostly random with the source region being around the extent of The Crab. The color bar is showing the test significance and is not in any units, the x-axis and y-axis are in galactic rising angle and declination respectively.

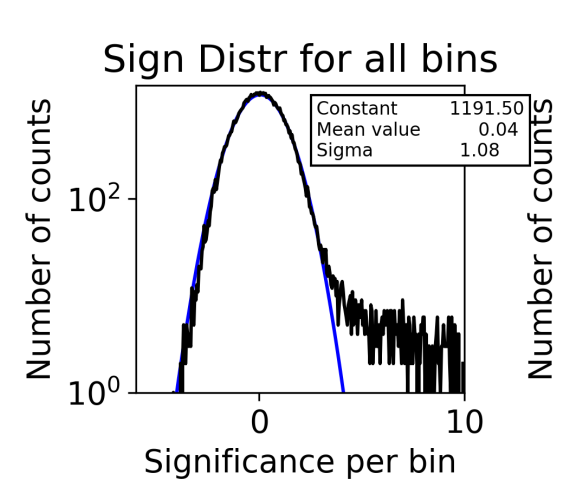


Figure 12: The Significance Plot produced by VEGAS for the Crab Nebula with a 0.7° exclusion region. The plot is shown with a fitted Gaussian. The plot's y-axis is the counts and the x-axis is the significance with units of nothing and sigma respectively.

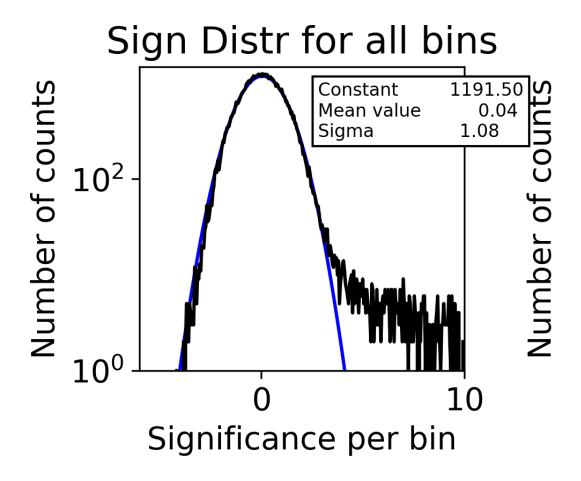


Figure 11: The Significance Plot produced by VEGAS for the Crab Nebula with a 0.4° exclusion region. The plot is shown with a fitted Gaussian. The plot's y-axis is the counts and the x-axis is the significance with units of nothing and sigma respectively.

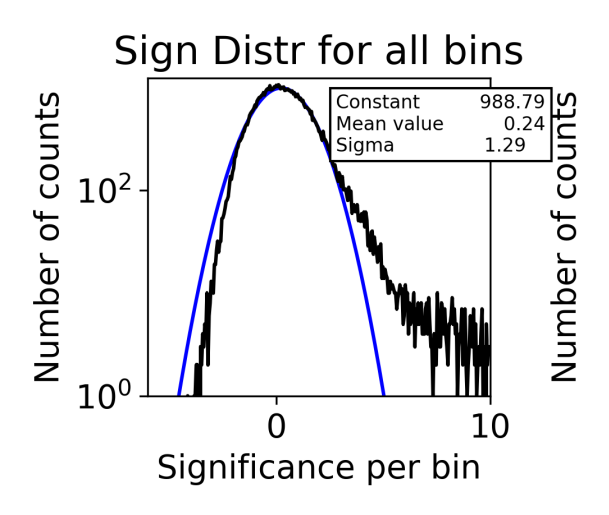


Figure 13: The Significance Plot produced by VEGAS for the Crab Nebula with a 0.9° exclusion region. The plot is shown with a fitted Gaussian, however the leftmost end of the graph shows a deviation of the gaussian from the data. The plot's y-axis is the counts and the x-axis is the significance with units of nothing and sigma respectively.

3.2. Results of validation with quasar 3C 273

The quasar 3C 273 is another point-like γ -ray source that is ideal for validation of the background estimation method. The same methods for the Crab Nebula were used to analyze 3C 273, but the exclusion regions 0.3° , 0.5° , 0.7° , and 0.9° were used as 3C 273 is much more dim than The Crab and thus can use a smaller initial exclusion region. From these points all of these same maps were produced but for the sake of brevity, only the 0.3° and 0.9° maps are shown in the main paper while the rest are included in the Appendix.

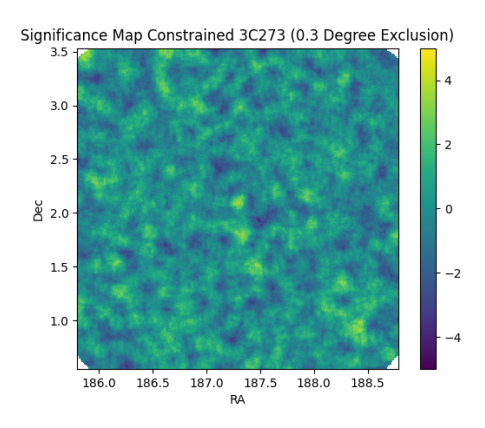


Figure 14: The Constrained Significance Map produced by VEGAS for 3C 273 with a 0.3° exclusion region. The color bar is showing the test significance and is not in any units, the x-axis and y-axis are in galactic rising angle and declination respectively.

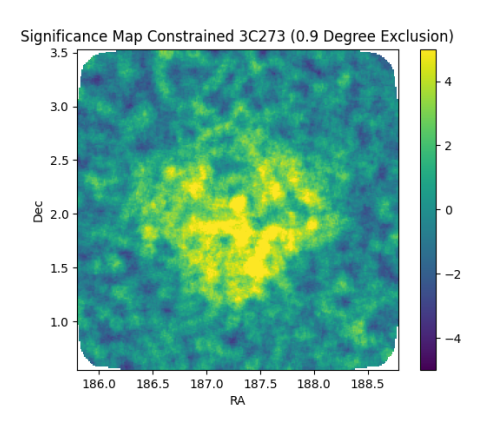


Figure 15: The Constrained Significance Map produced by VEGAS for 3C 273 with a 0.9° exclusion region. The color bar is showing the test significance and is not in any units, the x-axis and y-axis are in galactic rising angle and declination respectively.

From Figures 14 and 15 the same pattern is seen where the exclusion region becomes more significant because the background is not estimated well. There is large distinction between 0.3° and 0.9° where the background is failing, mostly in the center of the map. There is almost a detection of a large extended source at 0.9°, even though it is known that 3C 273 is a point source. This is also apparent when looking at the 1D significance distributions in Figures 16 and 17. From the 1D

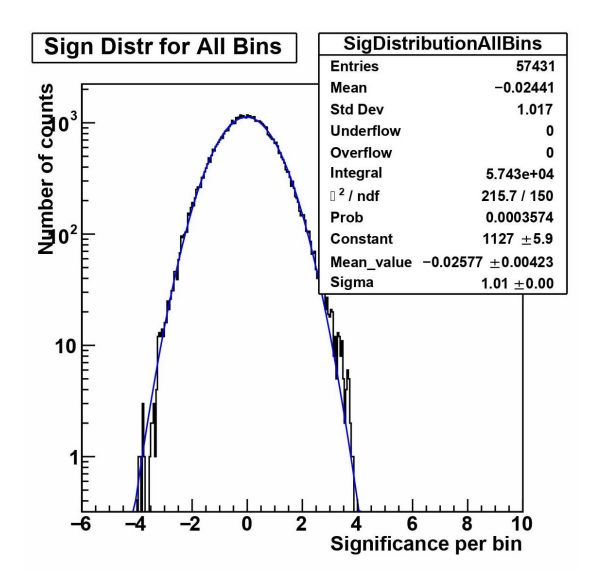


Figure 16: The 1D Significance Distribution for 3C 273 with a 0.3° exclusion radius. The plot is shown with a fitted gaussian. The x-axis and y-axis are in significance and counts respectively.

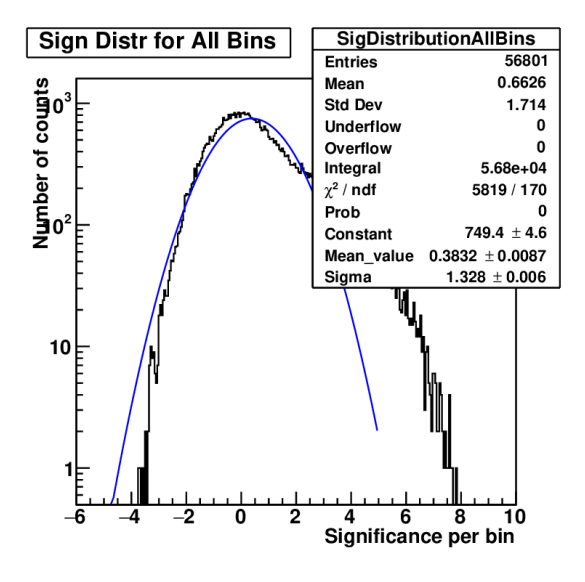


Figure 17: The 1D Significance Distribution for 3C 273 with a 0.9° exclusion radius. The plot is shown with a fitted gaussian. The x-axis and y-axis are in significance and counts respectively.

significance distributions it is clear that the data doesn't fit the nice gaussian distribution anymore. This is more evidence that the background estimation is failing.

4. Discussion

From the validation using the Crab and 3C 273, RBM estimation model starts to fail at a source exclusion region of 0.9°. There are two possible reasons for this. The first is that when the exclusion region is larger, the area that is being used for background estimation is of low statistics. Since there are less counts towards the edges, large error can occur when using that to predict the higher statistics in the center of the camera. It could also be that when the exclusion region is large, the background estimation is required to extrapolate over a larger region of angular space. This can then accrue large systematic uncertainty in the region which is being extrapolated.

5. Summary and conclusions

The field of γ -ray astronomy and the use of Imaging Atmospheric Cherenkov Telescopes (IACTs) have the potential to enhance our understanding of the processes that accelerate the most energetic cosmic rays. γ -rays originate in proximity to the locations where cosmic rays are born, hence their measurement can offer insights into these acceleration mechanisms. The recent catalog from the Large High Altitude Air Shower Observatory (LHAASO) reveals that many potential PeVatrons—astrophysical sources of ultra-high-energy cosmic rays—are extended sources. To accurately evaluate these sources, it is crucial to understand how background estimation functions for large exclusion regions, especially in relation to the Ring Background Method (RBM).

By analyzing data from the Crab Nebula and the quasar 3C 273, we discovered that the RBM requires further refinement for extended source analysis in regions beyond 0.9°. In addition, other aspects of the RBM, such as the ring width, may impact the analysis performance and thus warrant further investigation. Despite these challenges, several sources listed in the new LHAASO catalog, including HESS J1857+026 and its corresponding LHAASO source, have extensions below 0.9° and are viable candidates for analysis using the Very Energetic Radiation Imaging Telescope Array System (VERITAS).

The newly identified extended sources can provide unique and valuable data on cosmic ray acceleration mechanisms. The role of VERITAS in this research is essential, as it serves as a crucial instrument for multimessenger analysis. As more data from a range of experiments become available, we can corroborate conclusions regarding the acceleration processes in these astrophysical objects. This in turn, would enrich our knowledge about the workings of the universe.

Acknowledgements

This material is based upon work supported by the National Science Foundation under Grant No. PHY/1950431. Thanks to Professor Reshmi Mukherjee and Dr. Ruo Shang for assisting with the research done in this project. Thank you to Colin Adams and Jooyun Woo for their invaluable help with statistics, physical concepts, Python, and VEGAS. Thank you as well to the entire Nevis REU program as well as Dr. John Parson's, Dr. Georgia Karagiorgi, and Amy Garwood.

References

- [1] Cao, Z., Aharonian, F., An, Q., Axikegu, Bai, Y.X., Bao, Y.W., Bastieri, D., Bi, X.J., Bi, Y.J., Cai, J.T., Cao, Q., Cao, W.Y., Cao, Z., Chang, J., Chang, J.F., Chen, A.M., Chen, E.S., Chen, L., Chen, L., Chen, L., Chen, M.J., Chen, M.L., Chen, Q.H., Chen, S.H., Chen, S.Z., Chen, T.L., Chen, Y., Cheng, N., Cheng, Y.D., Cui, M.Y., Cui, S.W., Cui, X.H., Cui, Y.D., Dai, B.Z., Dai, H.L., Dai, Z.G., Danzengluobu, della Volpe, D., Dong, X.Q., Duan, K.K., Fan, J.H., Fan, Y.Z., Fang, J., Fang, K., Feng, C.F., Feng, L., Feng, S.H., Feng, X.T., Feng, Y.L., Gabici, S., Gao, B., Gao, C.D., Gao, L.Q., Gao, Q., Gao, W., Gao, W.K., Ge, M.M., Geng, L.S., Giacinti, G., Gong, G.H., Gou, Q.B., Gu, M.H., Guo, F.L., Guo, X.L., Guo, Y.Q., Guo, Y.Y., Han, Y.A., He, H.H., He, H.N., He, J.Y., He, X.B., He, Y., Heller, M., Hor, Y.K., Hou, B.W., Hou, C., Hou, X., Hu, H.B., Hu, Q., Hu, S.C., Huang, D.H., Huang, T.Q., Huang, W.J., Huang, X.T., Huang, X.Y., Huang, Y., Huang, Z.C., Ji, X.L., Jia, H.Y., Jia, K., Jiang, K., Jiang, X.W., Jiang, Z.J., Jin, M., Kang, M.M., Ke, T., Kuleshov, D., Kurinov, K., Li, B.B., Li, C., Li, C., Li, D., Li, F., Li, H.B., Li, H.C., Li, H.Y., Li, J., Li, J., Li, J., Li, K., Li, W.L., Li, W.L., Li, X.R., Li, X., Li, Y.Z., Li, Z., Li, Z., Liang, E.W., Liang, Y.F., Lin, S.J., Liu, B., Liu, C., Liu, D., Liu, H., Liu, H.D., Liu, J., Liu, J.L., Liu, J.Y., Liu, M.Y., Liu, R.Y., Liu, S.M., Liu, W., Liu, Y., Liu, Y.N., Lu, R., Luo, Q., Lv, H.K., Ma, B.Q., Ma, L.L., Ma, X.H., Mao, J.R., Min, Z., Mitthumsiri, W., Mu, H.J., Nan, Y.C., Neronov, A., Ou, Z.W., Pang, B.Y., Pattarakijwanich, P., Pei, Z.Y., Qi, M.Y., Qi, Y.Q., Qiao, B.Q., Qin, J.J., Ruffolo, D., Sáiz, A., Semikoz, D., Shao, C.Y., Shao, L., Shchegolev, O., Sheng, X.D., Shu, F.W., Song, H.C., Stenkin, Y.V., Stepanov, V., Su, Y., Sun, Q.N., Sun, X.N., Sun, Z.B., Tam, P.H.T., Tang, Q.W., Tang, Z.B., Tian, W.W., Wang, C., Wang, C.B., Wang, G.W., Wang, H.G., Wang, H.H., Wang, J.C., Wang, K., Wang, L.P., Wang, L.Y., Wang, P.H., Wang, R., Wang, W., Wang, X.G., Wang, X.Y., Wang, Y., Wang, Y.D., Wang, Y.J., Wang, Z.H., Wang, Z.X., Wang, Z., Wang, Z., Wei, D.M., Wei, J.J., Wei, Y.J., Wen, T., Wu, C.Y., Wu, H.R., Wu, S., Wu, X.F., Wu, Y.S., Xi, S.Q., Xia, J., Xia, J.J., Xiang, G.M., Xiao, D.X., Xiao, G., Xin, G.G., Xin, Y.L., Xing, Y., Xiong, Z., Xu, D.L., Xu, R.F., Xu, R.X., Xu, W.L., Xue, L., Yan, D.H., Yan, J.Z., Yan, T., Yang, C.W., Yang, F., Yang, F.F., Yang, H.W., Yang, J.Y., Yang, L.L., Yang, M.J., Yang, R.Z., Yang, S.B., Yao, Y.H., Yao, Z.G., Ye, Y.M., Yin, L.Q., Yin, N., You, X.H., You, Z.Y., Yu, Y.H., Yuan, Q., Yue, H., Zeng, H.D., Zeng, T.X., Zeng, W., Zha, M., Zhang, B.B., Zhang, F., Zhang, H.M., Zhang, H.Y., Zhang, J.L., Zhang, L.X., Zhang, L., Zhang, P.F., Zhang, P.P., Zhang, R., Zhang, S.B., Zhang, S.R., Zhang, S.S., Zhang, X., Zhang, X.P., Zhang, Y.F., Zhang, Y., Zhao, Y., Zhao, B., Zhao, J., Zhao, L., Zhao, L.Z., Zhao, S.P., Zhou, F., Zhou, B., Zhou, H., Zhou, J.N., Zhou, M., Zhou, P., Zhou, R., Zhou, X.X., Zhu, C.G., Zhu, F.R., Zhu, H., Zhu, K.J., Zuo., X., 2023. The first lhaaso catalog of gamma-ray sources. arXiv:2305.17030.
- [2] Griffiths, D.J., 2013. Introduction to electrodynamics. Pearson.
- [3] Karle, A., 2006. Gamma astronomy with ground based air cherenkov telescopes and other ground based detectors.
- [4] Li, T.P., Ma, Y.Q., 1983. Analysis methods for results in gamma-ray astronomy. 272, 317–324. doi:10.1086/161295.
- [5] Mukherjee, R., . Exploring the energetic universe with gamma-ray observatories.
- [6] Obodovskiy, I., 2019. Radiation , iiiURL: https://www.sciencedirect.com/science/article/pii/B97804446397900 doi:https://doi.org/10.1016/B978-0-444-63979-0.01001-6.
- [7] Petriella, A., Duvidovich, L., Giacani, E., 2021. Radio study of hess j1857+ 026: Gamma-rays from a superbubble? Astronomy & Astrophysics 652, A142.
- [8] Weekes, T.C., Cawley, M.F., Fegan, D., Gibbs, K., Hillas, A., Kowk, P., Lamb, R., Lewis, D., Macomb, D., Porter, N., et al., 1989. Observation of tev gamma-rays from the crab nebula using the atmospheric cherenkov imaging technique. Astrophysical Journal 342, 379–395.

Appendix A. More Plots

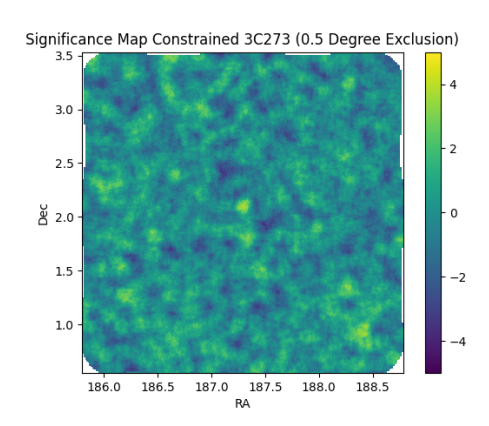


Figure A.18: The Constrained Significance Map produced by VEGAS for 3C 273 with a 0.5° exclusion region. The color bar is showing the test significance and is not in any units, the x-axis and y-axis are in galactic rising angle and declination respectively.

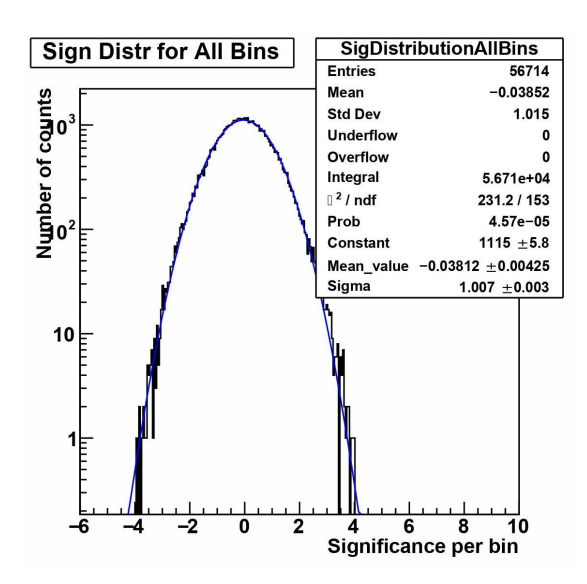


Figure A.20: The 1D Significance Distribution for 3C 273 with a 0.5° exclusion radius. The plot is shown with a fitted gaussian. The x-axis and y-axis are in significance and counts respectively.

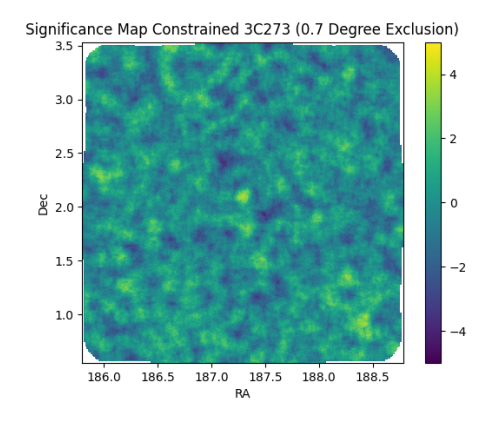


Figure A.19: The Constrained Significance Map produced by VEGAS for 3C 273 with a 0.7° exclusion region. The color bar is showing the test significance and is not in any units, the x-axis and y-axis are in galactic rising angle and declination respectively.

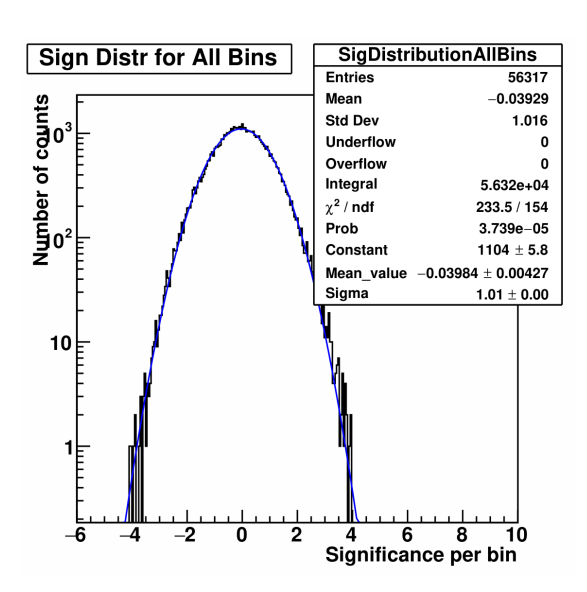


Figure A.21: The 1D Significance Distribution for 3C 273 with a 0.7° exclusion radius. The plot is shown with a fitted guassian. The x-axis and y-axis are in significance and counts respectively.